PHILOSOPHICAL TRANSACTIONS OF THE ROYAL SOCIETY A MATHEMATICAL, PHYSICAL & ENGINEERING SCIENCES

Singular Vectors and the Predictability of Weather and Climate

T. N. Palmer, R. Buizza, F. Molteni, Y.-Q. Chen and S. Corti

Phil. Trans. R. Soc. Lond. A 1994 **348**, 459-475
doi: 10.1098/rsta.1994.0105

Singular vectors and the predictability of weather and climate†

By T. N. Palmer[1], R. Buizza[1], F. Molteni[1], Y.-Q. Chen[2] and S. Corti[3]

[1] *European Centre for Medium-Range Weather Forecasts, Shinfield Park, Reading, Berkshire RG2 9AX, U.K.*

[2] *Joint Institute for the Study of the Atmosphere and Ocean, Department of Atmospheric Sciences, University of Washington, AK40, Seattle, Washington 98195, U.S.A.*

[3] *Department of Physics, University of Bologna, via Irnerio, Bologna 461-40126, Italy*

The local instability properties of a chaotic system are determined by the singular vectors and singular values of the dynamical evolution operator, linearized about a finite trajectory portion of the integral curves of the nonlinear equations. Knowledge of these quantities allows an assessment of the reliability of a finite-time forecast from a chaotic system.

After a brief study of the Lorenz model, singular vector analysis is applied to study three predictability issues in atmosphere–ocean dynamics. The first concerns the predictability of weather forecasts of a few days, and singular vector calculations are made from a large-dimensional numerical weather prediction model using an iterative Lanczos algorithm. The second concerns the predictability of El Niño on seasonal to interannual timescales. Here singular vector calculations are made using a coupled ocean–atmosphere model of the tropical Pacific region. Finally we show results from a multi-decadal integration of a medium-resolution quasi-geostrophic model, and discuss the possible relevance of singular vector analysis for the problem of climate change.

1. Introduction

The global instability characteristics of a chaotic system are, of course, determined by its positive Lyapunov exponents. They measure the asymptotic exponential divergence of initially close trajectories on the system's strange attractor; its climate.

Such attractors are not amorphous. The Lorenz (1963 *a*) attractor, for example, comprises two distinct régimes or 'butterfly wings'. This structure in turn induces inhomogeneity in the local phase-space divergence of trajectories. Knowledge of the local-phase space instability of a chaotic system allows an assessment of the reliability of a finite-time forecast from a chaotic system. Inhomogeneity of local

† This paper was produced from the authors' disk by using the TEX typesetting system.

Phil. Trans. R. Soc. Lond. A (1994) **348**, 459–475
Printed in Great Britain

phase-space predictability also affects the system's variable response to a fixed external forcing.

In this paper, we shall explore the use of singular vector analysis as a means of quantifying the local instability properties of a chaotic system. The singular vectors in question are of the dynamical evolution operator, linearized about a finite trajectory portion of the integral curves of the nonlinear equations. Unlike the eigenvectors of that operator, the singular vectors can usually be chosen to form an orthonormal basis for linear perturbations. The corresponding singular values give local divergence rates, and the singular vector with largest singular value represents the linear perturbation with largest growth over the trajectory portion. Unlike the Lyapunov exponents, the singular values do not necessarily describe exponential growth.

In § 2 we briefly describe some of the formalism of singular vector analysis and outline the close relations to more familiar energy-growth concepts: normal mode instability, upscale quasi-turbulent transfer, and the already-mentioned Lyapunov exponents.

In § 3, after a brief discussion of these concepts in the Lorenz model, we apply the analysis to three prediction problems in atmospheric–ocean dynamics. The first relates to forecasting the predictability of weather on timescales of a few days using complex numerical weather prediction models. The second relates to an analysis of the predictability of the El Niño phenomenon, during which equatorial Pacific sea surface temperatures warm by several degrees and disrupt the normal weather patterns over much of the globe on timescales of a few seasons. The El Niño is an irregular event, occurring every three or four years on average. Its prediction requires coupled ocean–atmosphere models. Finally, we discuss the possible relevance of singular vector analysis for the problem of climate change.

2. Basic formalism

We start by considering a general (M-dimensional) nonlinear evolution equation,

$$\mathrm{d}\boldsymbol{x}/\mathrm{d}t = \boldsymbol{A}[\boldsymbol{x}]. \tag{2.1}$$

For example, for the application of this analysis in § 3 *a*, (2.1) represents a complex numerical weather prediction model used at the European Centre for Medium-Range Weather Forecasts (ECMWF) (Simmons *et al.* 1989).

Consider a small perturbation $\boldsymbol{x}'$ of the state vector $\boldsymbol{x}$. For sufficiently short time intervals, its evolution can be described by the linearized approximation

$$\mathrm{d}\boldsymbol{x}'/\mathrm{d}t = \boldsymbol{A}_1\boldsymbol{x}' \tag{2.2}$$

of (2.1). $\boldsymbol{A}_1 \equiv (\mathrm{d}\boldsymbol{A}/\mathrm{d}\boldsymbol{x})|_{\boldsymbol{x}(t)}$ is the linear evolution operator evaluated on the nonlinear trajectory $\boldsymbol{x}(t)$.

Equation (2.2) can be written in the integral form

$$\boldsymbol{x}'(t) = \boldsymbol{L}(t, t_0)\boldsymbol{x}'(t_0). \tag{2.3}$$

The operator $\boldsymbol{L}(t, t_0)$ is referred to as the forward tangent propagator; it maps small perturbations along the (nonlinear) trajectory from an initial time t_0 to some future time t. From here on we drop the primes on the perturbation quantities. For the application to weather prediction, if $\boldsymbol{x}(t_0)$ is the typical error in

the initial conditions for a weather forecast, then (2.2) and (2.3) hold for approximately three days of integration time.

We now define an inner product $(\boldsymbol{x};\boldsymbol{y})$ based on total perturbation energy. By using (2.3) the perturbation norm at time t is given by

$$||\boldsymbol{x}(t)||^2 \equiv (\boldsymbol{x}(t);\boldsymbol{x}(t)) = (\boldsymbol{x}(t_0);\boldsymbol{L}^*\boldsymbol{L}\boldsymbol{x}(t_0)), \tag{2.4}$$

where $\boldsymbol{L}^*$ is the adjoint of $\boldsymbol{L}$ with respect to the energy inner product.

Unlike $\boldsymbol{L}$ itself, the operator $\boldsymbol{L}^*\boldsymbol{L}$ (sometimes referred to as the Oseledec operator (Abarbanel *et al.* 1991)) is symmetric. Hence its eigenvectors $\boldsymbol{\nu}_i(t_0)$ can be chosen to form a complete orthonormal basis in the M-dimensional tangent space of linear perturbations, with real eigenvalues $\sigma_i^2 \geqslant 0$ (see, for example, Noble & Daniel 1977), i.e.

$$(\boldsymbol{L}^*\boldsymbol{L})\boldsymbol{\nu}_i(t_0) = \sigma_i^2\boldsymbol{\nu}_i(t_0). \tag{2.5}$$

At future time t, these eigenvectors evolve to $\boldsymbol{\nu}_i(t) = \boldsymbol{L}\boldsymbol{\nu}_i(t_0)$, which in turn satisfy the eigenvector equation

$$(\boldsymbol{L}\boldsymbol{L}^*)\boldsymbol{\nu}_i(t) = \sigma_i^2\boldsymbol{\nu}_i(t). \tag{2.6}$$

From (2.4) and (2.5),

$$||\boldsymbol{\nu}_i(t)||^2 = (\boldsymbol{\nu}_i(t_0);\boldsymbol{L}^*\boldsymbol{L}\boldsymbol{\nu}_i(t_0)) = \sigma_i^2. \tag{2.7}$$

Because any $\boldsymbol{x}(t)/||\boldsymbol{x}(t_0)||$ can be written as a linear combination of the set $\boldsymbol{\nu}_i(t)$, it follows that

$$\max_{\boldsymbol{x}(t_0)\neq 0}(||\boldsymbol{x}(t)||/||\boldsymbol{x}(t_0)||) = \sigma_1. \tag{2.8}$$

Following the terminology of linear algebra, the σ_i, ranked in terms of magnitude, are here called the singular values of the operator $\boldsymbol{L}$ and the vectors $\boldsymbol{\nu}_i(t)$ are called the singular vectors of $\boldsymbol{L}$. Maximum energy growth over the time interval $t - t_0$ is therefore associated with the dominant singular vector: $\boldsymbol{\nu}_1(t_0)$ at initial time, and $\boldsymbol{\nu}_1(t)$ at optimization time.

Singular vector analysis is a generalization of classical normal mode instability analysis. This can be made explicit by linearizing about a stationary solution, so that normalized eigenvectors $\boldsymbol{\xi}_i$ of $\boldsymbol{A}_1$ with eigenvalues μ_i give rise to modal solutions $\boldsymbol{\xi}_i \exp[(t-t_0)\mu_i]$ of (2.2). The integral operator $\boldsymbol{L}(t,t_0)$ can be written as $\exp[(t-t_0)\boldsymbol{A}_1]$, with eigenvectors $\boldsymbol{\xi}_i$ and eigenvalues $\exp[(t-t_0)\mu_i]$.

For application to atmosphere–ocean dynamics, the linear evolution operators associated with realistic stationary basic state flows are generally not normal ($\boldsymbol{L}^*\boldsymbol{L} \neq \boldsymbol{L}\boldsymbol{L}^*$) because of vertical and horizontal shear. In this circumstance, normalized eigenvectors $\boldsymbol{\eta}_i$ and eigenvalues θ_i of the adjoint operator $\boldsymbol{L}^*$ satisfy the biorthogonality condition

$$(\mu_i - \theta_i^{cc})(\boldsymbol{\eta}_i, \boldsymbol{\xi}_i) = 0, \tag{2.9}$$

where cc denotes complex conjugate. This condition ensures that the eigenvalues of an eigenvector/adjoint eigenvector pair that are not orthogonal, must form a complex conjugate pair. The magnitude of the inner product $(\boldsymbol{\eta}_i, \boldsymbol{\xi}_i)$ for such eigenvector pairs depends on the angle, α_i, they subtend in phase space.

If an initial disturbance comprises a linear combination of the eigenvectors $\boldsymbol{\xi}_i$ so that

$$\boldsymbol{x}(t) = \sum_i c_i\boldsymbol{\xi}_i e^{\mu_i(t-t_0)}, \tag{2.10}$$

then from the biorthogonality condition (2.9)

$$c_i = (\boldsymbol{\eta}_i, \boldsymbol{x}(t_0))/(\boldsymbol{\eta}_i, \boldsymbol{\xi}_i). \tag{2.11}$$

From (2.10), the fastest growing normal mode will ultimately dominate the linear combination. Hence for sufficiently long optimization times, the dominant singular vector at optimization time will correspond to the most unstable normal mode. (Because the singular values are real, whilst the normal mode eigenvalues are complex, there is an arbitrary phase factor that has to be defined to make this correspondence precise.)

To maximize the contribution of the first normal mode at optimization time, c_1 in (2.10) should be as large as possible. If $\boldsymbol{x}(t_0)$ equals $\boldsymbol{\xi}_1$ then $c_1 = 1$, which could be highly sub-optimal. If fact, if $\boldsymbol{x}(t_0)$ projects onto $\boldsymbol{\eta}_1$, then c_1 is maximized and is given by the projectibility factor $1/(\cos\alpha_1)$ (Zhang 1988).

Hence, for indefinitely long optimization time, the dominant singular vector, at initial time, is determined by the first adjoint eigenvector, whereas the dominant singular vector at optimization time is determined by the first normal mode itself. The singular value will depend on both the e-folding time of the dominant normal mode and its projectibility. For finite optimization time the dominant singular vectors will no longer project onto individual normal mode solutions (and their adjoints), and the amplitude of finite-time instabilities need not be bounded by properties of the dominant normal modes alone.

If, instead of linearizing about a single stationary point on the climate attractor, we consider the other extreme of linearizing about a (time-evolving) trajectory portion which is sufficiently long to approximately cover the entire attractor, then according to the multiplicative ergodic theorem of Oseledec (1968) the singular values again have exponential dependence $\exp[(t - t_0)\lambda_i]$ on optimization time, where the Lyapunov exponents, λ_i, do not themselves depend on position on the attractor. The corresponding set of singular vectors $\boldsymbol{\nu}_i(t)$ can be referred to as the Lyapunov vectors. Note that although the Lyapunov exponents are themselves global quantities, the Lyapunov vectors are still defined locally, and thus vary with position on the attractor, and hence with time.

Singular vectors are, in general, not modal. For the application in § 3 *a*, their shape evolves not only in geographical space but also in the spectral distribution of energy. This spectral evolution describes, in a linear context, the upscale energy transfer associated with turbulent processes. To study this upscale energy transfer more explicitly we introduce a spectral projection operator $\boldsymbol{P}_{[n_1,n_2]}$, where $[n_1, n_2]$ denotes the total wavenumber interval $n_1 \leqslant n \leqslant n_2$. $\boldsymbol{P}_{[n_1,n_2]}$ is defined as

$$\boldsymbol{P}_{[n_1,n_2]}\boldsymbol{x}_n = \begin{cases} \boldsymbol{x}_n & \text{if } n \in [n_1, n_2], \\ 0 & \text{otherwise.} \end{cases} \tag{2.12}$$

Here $\boldsymbol{x}_n$ is the wavenumber n component of the spherical harmonic expansion of the (atmospheric) state vector. If we wish to find perturbations, initially constrained to be in $[n_3, n_4]$, with maximum energy in $[n_1, n_2]$, these are given by the singular vectors of $\boldsymbol{P}_{[n_1,n_2]}\boldsymbol{L}\boldsymbol{P}_{[n_3,n_4]}$.

When systems with a large number of degrees of freedom (e.g. $O(10^4)$ or more) are considered, the eigenvalue problem (2.5) and (2.6) cannot be solved using conventional matrix algorithms. However, iterative techniques provide an alternative possibility if the adjoint propagator has been coded. The power method, whereby a random initial vector is operated on repeatedly by $\boldsymbol{L}^*\boldsymbol{L}$, is an example. A more sophisticated technique such as the Lanczos algorithm (Strang 1986) is required if more than the largest singular vector is required.

3. Applications of singular vector analysis

(*a*) *The Lorenz model*

The first application of the above formalism is to the prototype dissipative chaotic system: the Lorenz (1963*a*) model

$$\dot{X} = -\sigma X + \sigma Y, \tag{3.1a}$$

$$\dot{Y} = -XZ + rX - Y, \tag{3.1b}$$

$$\dot{Z} = XY - bZ, \tag{3.1c}$$

Figure 1 shows the familiar Lorenz attractor, superimposed on which are three ensembles of points integrated from initial conditions on different parts of the attractor. The dispersion of the ensemble identifies the origin as a region of particular unpredictability.

Singular values for the Lorenz model have been computed by a number of authors (see, for example, Mukougawa *et al.* 1991; Abarbanel *et al.* 1991; Trevisan 1993). Figure 2 shows the distribution of exponents of dominant singular values for two choices of the trajectory length. For relatively long trajectory portions, the distribution of singular values is relatively narrow and is clearly asymptoting to the appropriate largest Lyapunov exponent (here about 1.5). For short trajectory portions the distribution of maximum exponents is broad, varying from negative values (i.e. decaying singular vectors) to values over one order of magnitude greater than the fastest growing Lyapunov exponent.

Figure 3*a* shows the state vector probability density function (PDF) of the Lorenz model computed from a long integration. It is effectively symmetric with maxima corresponding to the centroids of the butterfly-wing régimes. In figure 3*b* a constant forcing $F = 1/\sqrt{2}$ is applied to the right-hand side of (3.1*a*, *b*). The system continues to be chaotic, though the PDF is now biased to one of the régimes; however, the phase space position of the régime centroids remains essentially unchanged. This behaviour can be understood by noting that the influence of F on the state vector is greatest near the origin where the dominant singular value is large (see, for example, Palmer 1993).

These simple properties of the Lorenz model have some correspondence with more complex models of the atmosphere and oceans; see below.

(*b*) *A numerical weather prediction model*

We discuss here results from a complex primitive equation numerical weather prediction model used at ECMWF (Simmons *et al.* 1989). The adjoint of this model has been coded (Courtier *et al.* 1991), and estimation of the first 20 or so singular vectors, optimized over periods of a few days, are possible using an iterative Lanczos technique. See Buizza & Palmer (1994) for details. The singular vector calculations described here are made using 19 vertical levels with triangular truncation at either wavenumber 21 or wavenumber 42.

We discuss some of the characteristics of atmospheric singular vectors from a particular case study. During the period under question (9–12 January 1993), there was a vigorous east–west oriented flow across the north Atlantic associated with strong baroclinity. (During this period the oil tanker Braer was grounded on the Shetland Island during heavy storms (Mansfield 1993).)

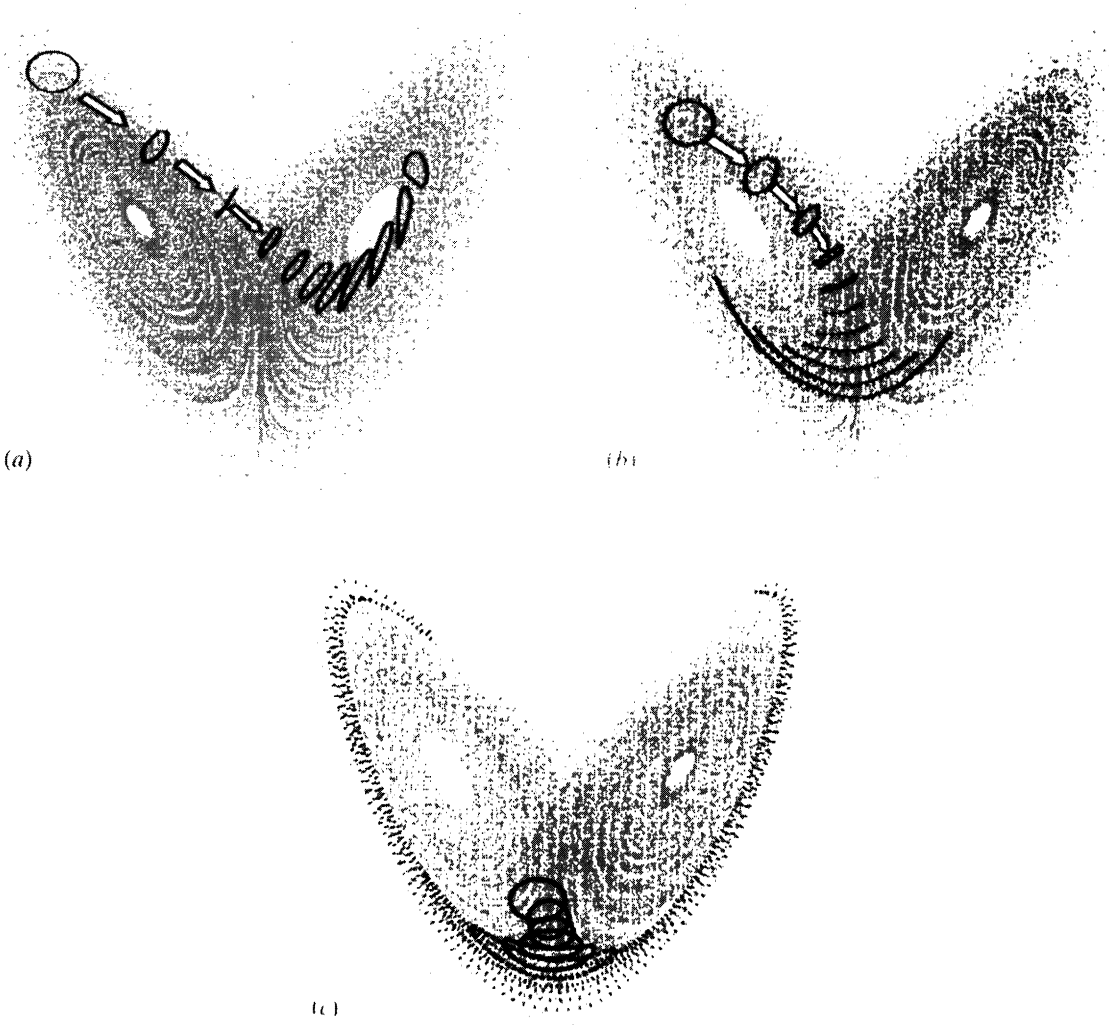

Figure 1. Phase-space evolution of an ensemble of initial points on the Lorenz attractor, for three sets of initial conditions.

Figure 4 shows the dominant singular vector calculated using the primitive equation model, for a three day trajectory portion made from initial conditions on 9 January 1993, at three levels in the atmosphere (200 hPa, 700 hPa and 850 hPa) at initial and optimization time. The figure illustrates features which bear qualitative resemblance to idealized normal-mode baroclinic instability (Charney 1947; Eady 1949): the disturbance clearly amplifies at is propagates through the region of maximum baroclinity (where north–south temperature gradients are strongest), and the disturbance shows evidence of westward tilting phase with height, consistent with a northward flux of heat.

On the other hand, the figure also clearly illustrates the non-modal nature of the disturbance and is qualitatively similar in some respects to idealized non-modal optimal baroclinic excitation described by Farrell (1989). At initial time

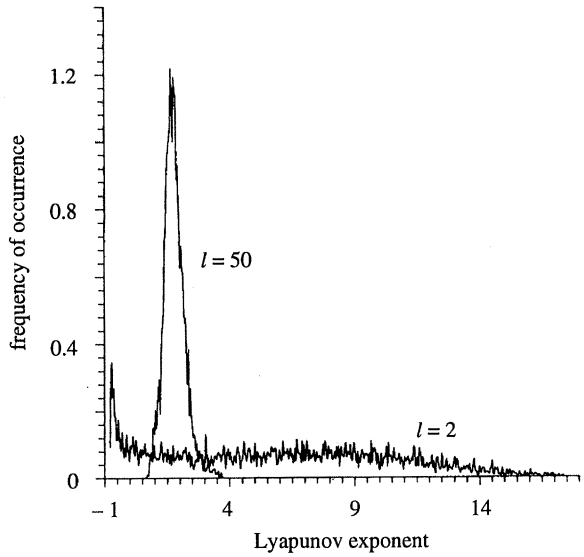

Figure 2. The distribution of the largest singular value, σ, (shown as its exponent $\ln\sigma$ for the Lorenz model (3.1) for two trajectory lengths $L = 2$, $L = 50$. Each distribution is normalized to unity. From Abarbanel *et al.* (1991).

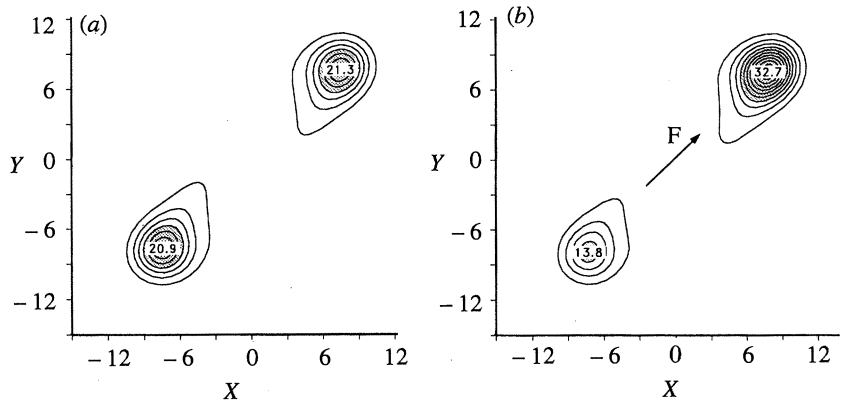

Figure 3. PDF of the Lorenz model in the XY plane, low-pass filtered to remove oscillations around a régime centroid (a) from the unforced model (b) with a constant forcing $F_X = F_Y = 1/\sqrt{2}$, $F_Z = 0$.

the disturbance is localized near the north Atlantic jet entrance region; at optimization time the disturbance has propagated downstream to Europe. At initial time, maximum disturbance amplitude is located in the lower troposphere, whilst at optimization time maximum amplitude is located in the upper troposphere at the level of maximum winds (understandable qualitatively using wave-activity conservation concepts; see Buizza & Palmer 1994). Finally, the horizontal scale of the initial disturbance is noticeably smaller at initial time than at optimization time.

This final aspect of non-modality is explored further in figure 5 which shows the energy distribution of the singular vector at initial and final time, as a function of

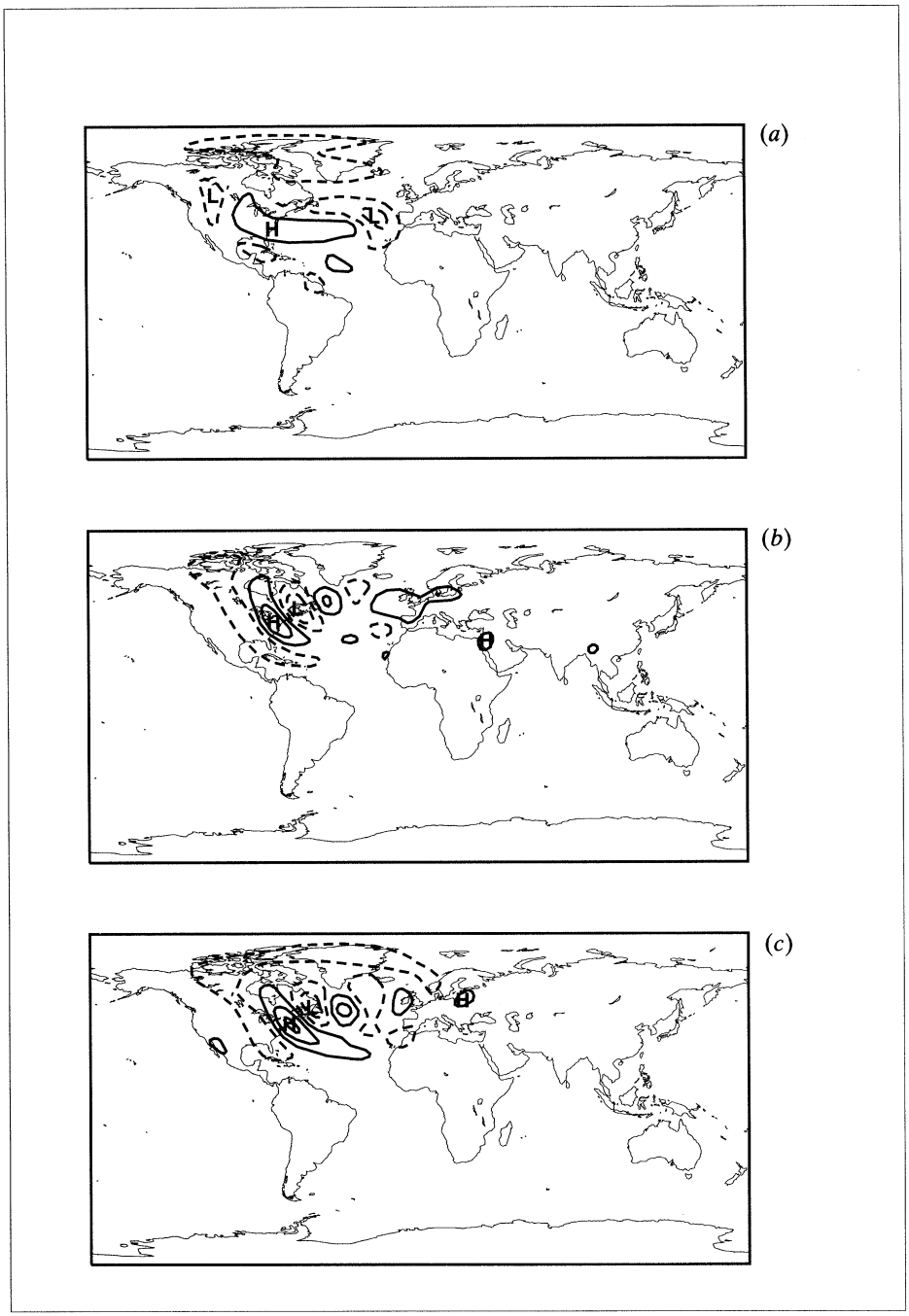

Figure 4. (*a*)–(*c*) For description see opposite.

PHILOSOPHICAL TRANSACTIONS OF THE ROYAL SOCIETY A MATHEMATICAL, PHYSICAL & ENGINEERING SCIENCES

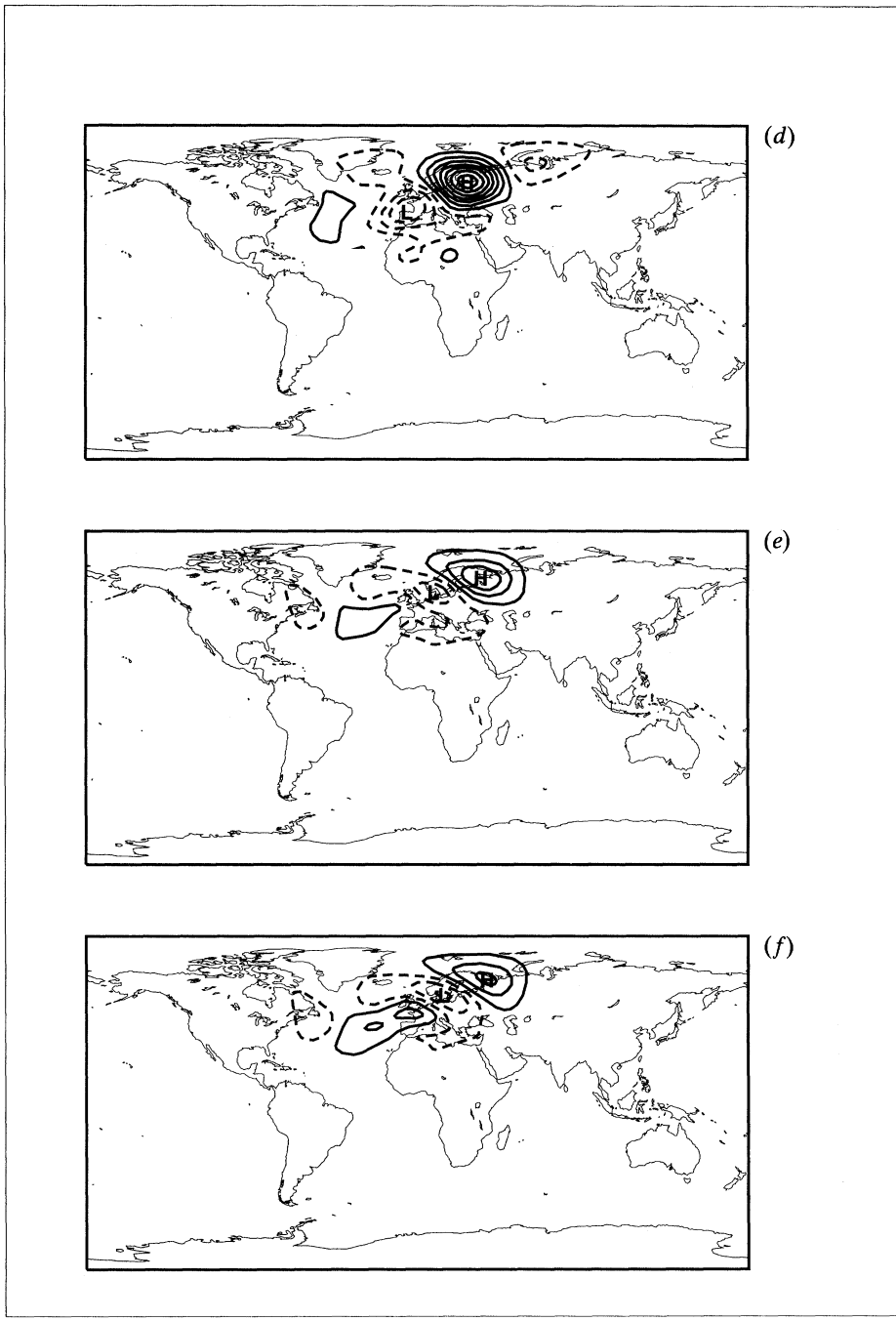

Figure 4. Streamfunction of the dominant atmospheric singular vector calculated using a primitive equation numerical weather prediction model for a three-day trajectory portion made from initial conditions of 9 January 1993 at three levels (200 hPa (*a*), (*d*), 700 hPa (*b*), (*e*), 850 hPa (*c*), (*f*)). Panels (*a*)–(*c*) show initial time. Panels (*d*)–(*f*) show optimization time. Contour interval at optimization time is 20 times larger than at initial time.

PHILOSOPHICAL TRANSACTIONS OF THE ROYAL SOCIETY A MATHEMATICAL, PHYSICAL & ENGINEERING SCIENCES

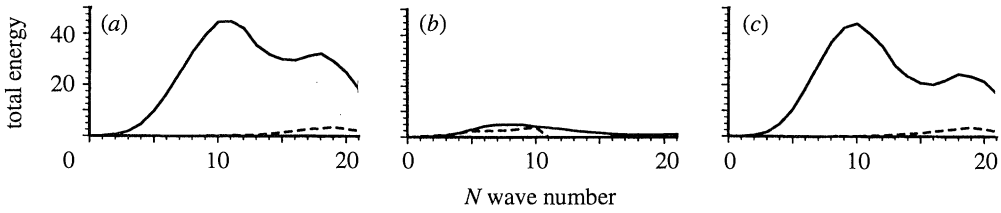

Figure 5. Energy distribution of three-day singular vector from 9 January 1993 as a function of (total) wavenumber. Dashed lines show initial time with values multiplied by 20 in order to be visible. Solid lines show optimization time. (*a*) For singular vector shown in figure 4. (*b*) For singular vector with energy optimized for wavenumbers 0–10, and constrained to wavenumbers 0–10 at initial time. (*c*) For singular vector with energy optimized for wavenumbers 0–10, and constrained to wavenumbers 11–20 at final time.

total wavenumber. Figure 5*a* shows the spectral distribution of the disturbance shown in figure 4 peaking near the truncation limit at initial time (dashed line) and at about wavenumber 10 at optimization time. This upscale energy transfer can occur because the basic state (unlike those in many idealized calculations) is itself an unrestricted solution to the equations of motion, and in particular contains scales comparable with those in the disturbance field. This allows triad interactions between two disturbance scales and a third trajectory scale.

Figure 5*b*, *c* shows the spectral distribution of two further singular vector calculations made using this trajectory. In these further calculations, the spectral projection operator has been applied both at initial and optimization time. For both calculations the operator at optimization time maximizes energy between wavenumbers 0 and 10. The initial perturbation is constrained at wavenumbers 0–10 in figure 5*b* and at wavenumbers 11–20 in figure 5*c*.

The results are quite dramatic. Constraining the perturbation to have the same energy distribution in wavenumber space at initial and final time (which a normal mode solution, if it exists, must have), severely restricts perturbation growth. On the other hand, constraining the perturbation at initial and final time to have energy in non-overlapping wavenumber intervals hardly restricts energy growth at all.

The result of this calculation illustrates the butterfly effect in its original sense (Lorenz 1963*b*), i.e. that small-scale initial disturbances will ultimately have an overwhelming influence on large-scale disturbances. This is in addition to the commonly perceived meaning of the butterfly effect that small-amplitude initial disturbances will ultimately have an overwhelming effect on large-amplitude disturbances. (In fact, Lorenz refers to the influence on the weather of a flap of a sea-gull's rather than a butterfly's wings. In view of the location of the initial singular vectors over the west Atlantic ocean, rather than, say, over Amazonia, this original metaphor is fortuitously appropriate!)

At ECMWF singular vectors from these primitive equation calculations are now routinely used to construct initial perturbations for 10-day ensemble forecasts. Each ensemble comprises 33 individual forecasts. Within an ensemble, each individual forecast essentially integrates a singular vector beyond the range for which the linear approximation is valid (about 3 days). Figure 6 shows the ensemble dispersion of two ensemble forecasts made one week apart. The first example shows large dispersion, the second small. From a practical point of view a weather forecaster would be warned that any single deterministic prediction from the first

PHILOSOPHICAL TRANSACTIONS OF THE ROYAL SOCIETY A MATHEMATICAL, PHYSICAL & ENGINEERING SCIENCES

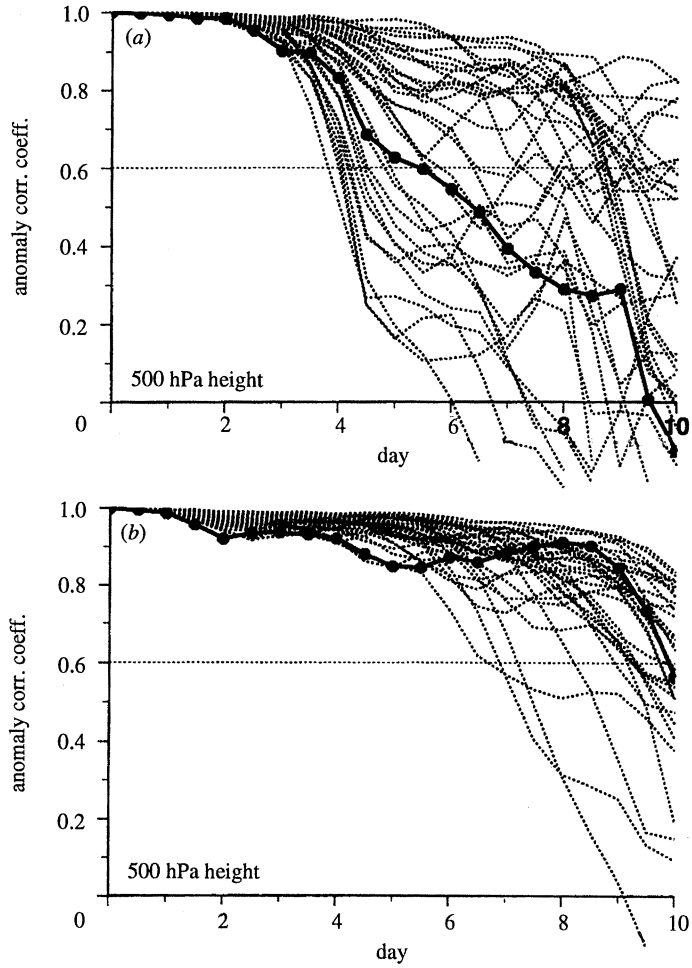

Figure 6. Ten-day ensemble forecast dispersion as measured by anomaly correlation between 500 hPa geopotential height of control and perturbed forecasts, over Europe (light lines). Skill of 10-day control forecast (heavy line), (*a*) forecasts from 30 October 1993, (*b*) forecasts from 13 November 1993.

example is unlikely to be reliable, whereas any prediction from the second example is likely to be relatively skilful. The skill of the operational ECMWF forecast is also shown for these two cases confirming the ensemble predictions of reliability. Using these ensemble predictions, ECMWF now routinely issues dynamically based probabilistic weather forecasts out to 10 days.

From a meteorological point of view, both cases in figure 6 involved a transition in flow type. In some sense these mimic ensemble predictions (figure 1 *c*, *a*) in the Lorenz model, which also showed unpredictable and predictable régime transitions.

(*c*) *A coupled tropical ocean–atmosphere model*

There is currently much excitement in the climate community about the feasibility of making predictions about the natural year-to-year fluctuations of the

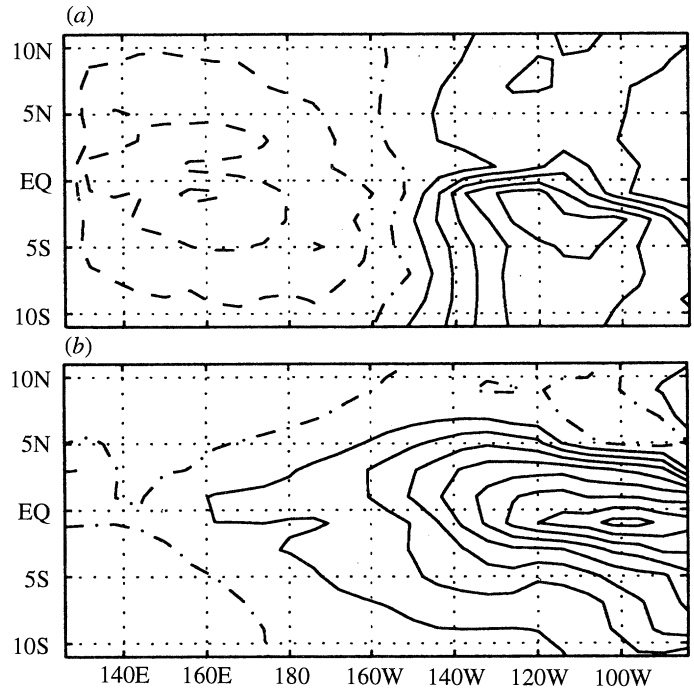

Figure 7. Sea surface temperature of a dominant six-month singular vector at initial, (*a*), and optimization, (*b*), time from a coupled ocean–atmosphere model of the tropical Pacific. Starting conditions are in April, and the basic state is constructed from climatology.

climate system. Much of this excitement has stemmed from the demonstration that the El Niño/Southern Oscillation phenomenon is predictable up to a year or so in advance using relatively simple numerical models of the atmosphere and ocean coupled together (Zebiak & Cane 1987). El Niño is the name given to an irregular oscillation in the sea surface temperature of the tropical Pacific ocean. The Southern Oscillation denotes a corresponding atmospheric perturbation in the surface pressure field above the equatorial Pacific. According to Münnich *et al.* (1991), long-term variability of the El Niño/Southern Oscillation phenomenon is intrinsically chaotic (independent of the chaotic nature of weather itself).

It is known that during years in which the El Niño phenomenon is active, much of the world's weather patterns are significantly disturbed, leading to drought in some parts of the world, floods in other parts and to overall global warming (IPCC 1992). For example, the warming in surface temperature averaged over the Northern Hemisphere is related to the existence of atmospheric teleconnections arising from exitation of atmospheric planetary-scale wave patterns by anomalous latent-heat release over the El Niño area closely related to the patterns shown in figure 8. These teleconnections lead to a bias in extratropical régime (or weather-pattern) statistics, similar to that shown in figure 3*b* for the Lorenz model.

The skill of El Niño forecasts made with coupled ocean–atmosphere models is seasonally dependent (Cane *et al.* 1986). Typically, seasonal forecasts beginning in spring tend to be less skilful than forecasts beginning, for example, in autumn. Blumenthal (1991) has analysed the behaviour of the eigenfunctions of a linear

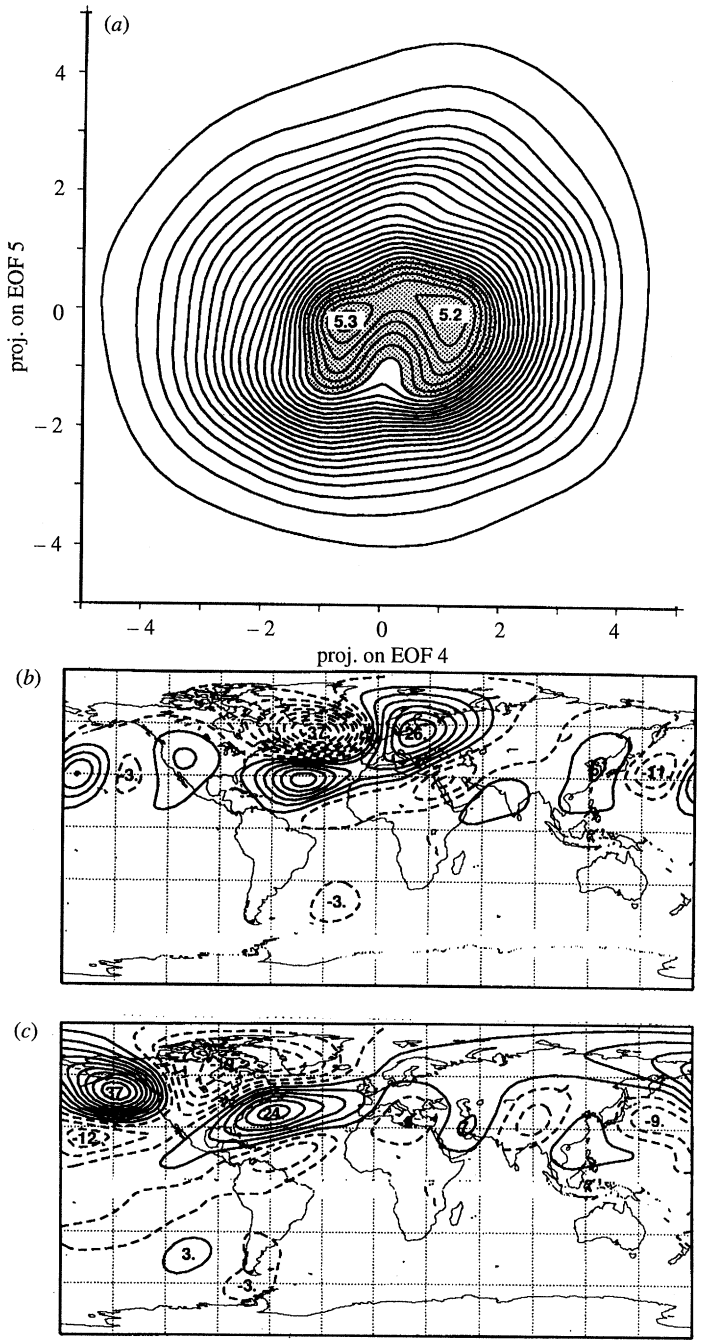

Figure 8. (*a*) Two-dimensional cut of the PDF from 100 consecutive winters of a multi-decadal integration in a T21L3 quasi-geostrophic model. (*b*), (*c*) The empirical orthogonal functions from the model, used to define the axes in (*a*). The PDF is bimodal along the axis given by (*b*).

PHILOSOPHICAL TRANSACTIONS OF THE ROYAL SOCIETY A MATHEMATICAL, PHYSICAL & ENGINEERING SCIENCES

Markov model approximation to a nonlinear coupled ocean–atmosphere model. He finds that in summer the eigenfunction best describing the El Niño oscillation has a larger eigenvalue than at other times of year. On the other hand, in spring this El Niño eigenfunction is least orthogonal to other modes, i.e. is associated with large projectibility (see § 2). Error growth in spring appears therefore to be strongly associated with non-self-adjoint energy growth. Both types of error growth (normal and non-normal) are implicit in singular vector analysis.

We show some preliminary results of a singular vector analysis applied to the coupled ocean–atmosphere model of Battisti (1988). The ocean component of this model is a single vertical mode tropical Pacific basin anomaly model, governed by linear shallow water wave dynamics. The nonlinear thermodynamics are only active in a surface mixed layer. The atmospheric component is a thermally forced steady linear model with single vertical mode (Gill 1980). Air–sea interactions are nonlinear, given by surface wind stress, heat flux, and sea surface temperature (SST). The number of independent degrees of freedom in the coupled model is reduced to 420 by considering only the equatorial oceanic Kelvin mode, and first three symmetric Rossby modes. With such a reduction, singular vectors can be computed using conventional matrix algorithms.

Calculations described here are performed for six-month optimization times, linearized about a climatological basic state. The optimization time is greater than in § 3*b* because of the longer predictability of this coupled atmosphere–ocean oscillation. Singular vector calculations were made starting in April and October, and are based on maximizing sea surface temperature variance.

For the April start, the dominant singular value is 6.22. The structure of the sea surface temperature of this vector at initial and optimization time is shown in figure 7. It illustrates non-modal growth consistent with the analyses of Blumenthal (1991) and Xue *et al.* (1994). At initial time there is an east-west dipole in sea surface temperature perturbation; this evolves to a monopole structure in the eastern Pacific similar to the mature El Niño event itself. By contrast, the dominant singular value for the October start is only 1.96.

According to the results described here, errors in the measurement of sea surface temperature in the tropical Pacific (inevitable given the limited data in that area) would have a significant impact on the accuracy of a six-month forecast of the El Niño event for forecasts beginning around springtime; less so for forecasts beginning in autumn.

In these calculations, the basic state has been constructed from climatology. More generally the predictability of tropical Pacific sea surface temperature is a function of the actual ocean–atmosphere state, particularly with respect to the El Niño oscillation. As with the calculations in § 3 *b*, these oceanic singular vectors can be readily generalized to include observed variations in basic-state flow. Such calculations are in progress.

(*d*) *Climate change*

One atmospheric forecast which has attracted more attention worldwide by governments and the public alike, is of a trend to warmer temperatures as anthropogenic greenhouse gases, such as CO_2, increase. Such warming necessarily occurs in a one-dimensional radiative equilibrium atmosphere without dynamics. However, one can ask the question of how chaotic nonlinear dynamics may compromise such radiative equilibrium calculations.

As discussed in § 3 *a*, for the Lorenz model, the impact of a small externally imposed forcing on a dynamical system is potentially greater on parts of the attractor where singular values are large. On the other hand the response to this forcing, given by changes in the system PDFs, may be largely determined by the values of the PDFs at régime centroids, well removed (in phase-space) from regions of maximum instability. Whether the response to the imposed forcing is an increase in the frequency of one régime rather than another, may depend quite strongly on the local attractor geometry in the regions of strong instability.

In principle it would be possible to run the primitive equation model above over long climatic periods of time, and obtain detailed knowledge of the structure of the climate attractor, and associated estimates of the singular-vector structure of this attractor. However, this is overwhelmingly too computationally expensive at present. On the other hand, excessive truncation of the atmospheric equations of motion (say to less that 100 degrees of freedom) produces results which may depend excessively on quasi-resonant properties of low-order models.

However, it is now feasible to run quasi-geostrophic models with reasonable resolution over century periods of time, and compute local singular vector structures. Figure 8*a* shows the PDF from a 100 consecutive winter sample of a 1200 perpetual winters integration of a 3-level T21 quasi-geostrophic model (Marshall & Molteni 1993). Singular vectors from this model can be estimated using conventional matrix eigenvector techniques (Molteni & Palmer 1993). The PDF is estimated in a phase-space plane spanned by two of the dominant empirical orthogonal functions of the model. It can be seen that the PDF during this chosen period is bimodal along an axis that corresponds to the intensity of the north Atlantic jet (figure 8*b*). These two model régime centroids would generate different surface temperature fields, both over the Atlantic and Europe. (In fact the calculations described in § 3 *b* were made when the atmosphere was in one of these régimes with strong north Atlantic westerlies.) The impact of a small external forcing would lead to either an increase or decrease in one régime over another. Which one increases may depend crucially on the geometry of the attractor at some possible unstable saddle point between the régimes. As such, the fact that one régime is associated with warmer temperatures than the other is not directly relevant in determining whether its PDF increases or decreases. Calculation of singular vectors associated with finite trajectory portions that make up the PDF in figure 7*a* are currently under way.

These general remarks also apply to considerations of changes to global temperature. For example, as mentioned above, global-mean temperature tends to be warmer than average during years in which the El Niño event is active. If the impact of enhanced greenhouse gases was to alter the frequency of El Niño events, then over decadal and longer timescales, this would contribute to a component of global climate change. We have briefly discussed the structure and growth of singular vectors in the tropical Pacific that lead to El Niño. Projection of radiative forcing from enhanced CO_2 onto these geographically localized singular vectors (particularly during the northern spring and summer) may be critical in determining this component of global temperature change.

These considerations are, of course, implicit in the calculations of climate change made with our best comprehensive global circulation models (IPCC 1992). These models consistently predict global warming, qualitatively similar to the radiative equilibrium calculations. The models are our best hope at quantifying cli-

PHILOSOPHICAL TRANSACTIONS OF THE ROYAL SOCIETY A MATHEMATICAL, PHYSICAL & ENGINEERING SCIENCES

mate change, and their predictions must therefore treated seriously. On the other hand, such models are not free of systematic error; not least they are generally poor in simulating the observed statistics of the El Niño/Southern Oscillation phenomenon. Analysis of the processes by which atmosphere–ocean dynamics influence climate is an important component of research on climate change.

4. Conclusions

We have described the formalism of singular vector analysis which allows one to study local phase-space instability of inhomogeneous chaotic attractors. Using adjoint models and iterative eigenvector solvers, we are able to apply the formalism to large-dimensional systems. In this paper we have applied the method to the study of the predictability of weather and climate. However, in principle, the techniques may also be of use in studies of the predictability of other large-dimensional chaotic systems as occur, for example, in the natural sciences, engineering, economics and elsewhere.

References

Abarbanel, H. D. I., Brown, R. & Kennel, M. B. 1991 Variation of Lyapunov exponents on a strange attractor. *J. Nonlinear Sci.* **1**, 175–199.

Battisti, D. S. 1988 Dynamics and thermodynamics of a warming event in a coupled tropical atmosphere–ocean model. *J. atmos. Sci.* **45**, 2889–2919.

Blumenthal, B. 1991 Predictability of a coupled ocean–atmosphere model. *J. Climate* **4**, 766–784.

Buizza, R. & Palmer, T. N. 1994 The singular vector structure of the atmospheric general circulation. *J. atmos. Sci.* (In the press.)

Cane, M. A., Zebiak, S. & Dolan, S. 1986 Experimental forecasts of El Niño. *Nature, Lond.* **321**, 827–832.

Charney, J. G. 1947 The dynamics of long waves in a baroclinic westerly current. *J. Meteor.* **4**, 135–163.

Courtier, P., Freydier, C., Geleyn, J.-F., Rabier, F. & Rochas, M. 1991 The Arpege project at Météo, France. In *Proc. ECMWF Seminar on Numerical methods in atmospheric models*, vol. 2, pp. 193–231. Reading, U.K.: ECMWF.

Eady, E. T. 1949 Long waves and cyclone waves. *Tellus* **1**, 33–52.

Farrell, B. F. 1989 Optimal excitation of baroclinic waves. *J. atmos. Sci.* **46**, 1193–1206.

Gill, A. E. 1980 Some simple solutions for heat-induced tropical circulation. *Q. Jl R. met. Soc.* **106**, 447–462.

IPCC 1992 *Climate change, the supplementary report to the IPCC scientific assessment.* Cambridge University Press.

Lorenz, E. N. 1963 *a* Deterministic nonperiodic flow. *J. atmos. Sci.* **20**, 130–141.

Lorenz, E. N. 1963 *b* The predictability of hydrodynamic flow. *Trans. New York Acad. Sci. 2* **25**, 409–432.

Mansfield, D. A. 1993 The storm of 10 January 1993. *Met. Mag.* **122**, 140–146.

Marshall, J. & Molteni, F. 1993 Toward a dynamical understanding of planetary-scale flow régimes. *J. atmos. Sci.* **50**, 1792–1818.

Molteni, F. & Palmer, T. N. 1993 Predictability and finite-time instability of the northern winter circulation. *Q. Jl R. met. Soc.* **119**, 269–298.

Mukougawa, H., Kimoto, M. & Yoden, S. 1991 A relationship between local error growth and quasi-stationary states in the Lorenz system. *J. atmos. Sci.* **48**, 1231–1237.

PHILOSOPHICAL TRANSACTIONS OF THE ROYAL SOCIETY A MATHEMATICAL, PHYSICAL & ENGINEERING SCIENCES

Münnich, M., Cane, M. A. & Zebiak, S. E. 1991 A study of self-excited oscillations in a tropical ocean–atmosphere system. Part II: Nonlinear cases. *J. atmos. Sci.* **48**, 1238–1248.

Noble, B. & Daniel, J. W. 1977 *Applied linear algebra.* Prentice-Hall.

Oseledec, V. I. 1968 A multiplicative ergodic theorem. Lyapunov characteristic numbers for dynamical systems. *Trudy Mosk. Mat. Obsc.* **19**, 197.

Palmer, T. N. 1993 Extended-range atmospheric prediction and the Lorenz model. *Bull. Am. met. Soc.* **74**, 49–65.

Simmons, A. J., Burridge, D. M., Jarraud, M., Girard, C. & Wergen, W. 1989 The ECMWF medium-range prediction models development of the numerical formulations and the impact of increased resolution. *Meteorol. atmos. Phys.* **40**, 28–60.

Strang, G. 1986 *Introduction to applied mathematics.* Wellesley-Cambridge Press.

Trevisan, A. 1993 Impact of transient error growth on global average predictability measures. *J. atmos. Sci.* **50**, 1016–1028.

Xue, Y., Cane, M. A., Zebiak, S. E. & Blumenthal, M. B. 1994 On the prediction of ENSO. A study with a low order Markov. *Tellus.* (In the press.)

Zebiak, S. E. & Cane, M. A. 1987 A model El Niño–Southern Oscillation. *Mon. Wea. Rev.* **115**, 2262–2278.

Zhang, Z. 1988 The linear study of zonally asymmetric barotropic flows. Ph.D. thesis, University of Reading, U.K.

PHILOSOPHICAL TRANSACTIONS OF THE ROYAL SOCIETY A MATHEMATICAL, PHYSICAL & ENGINEERING SCIENCES

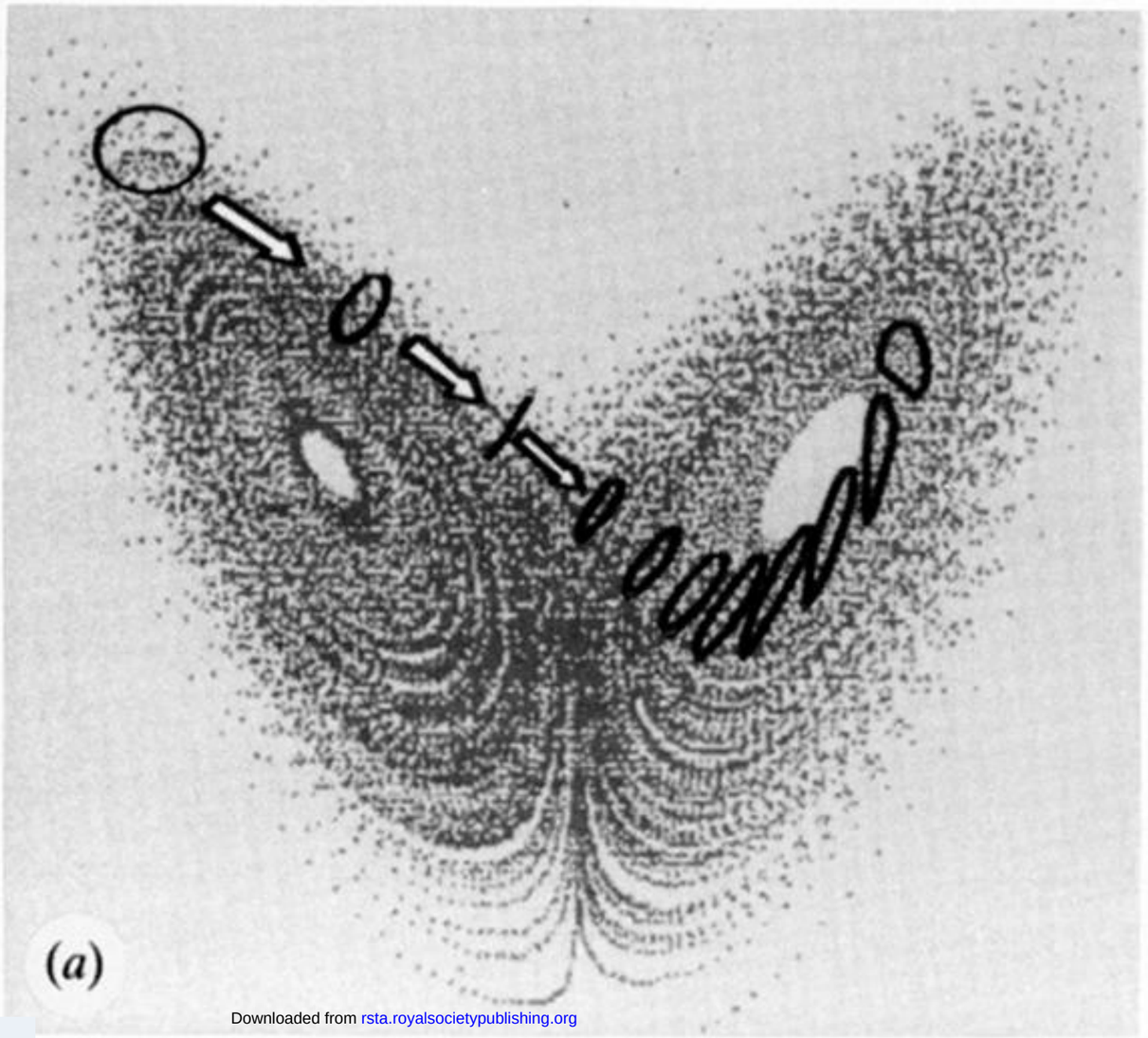

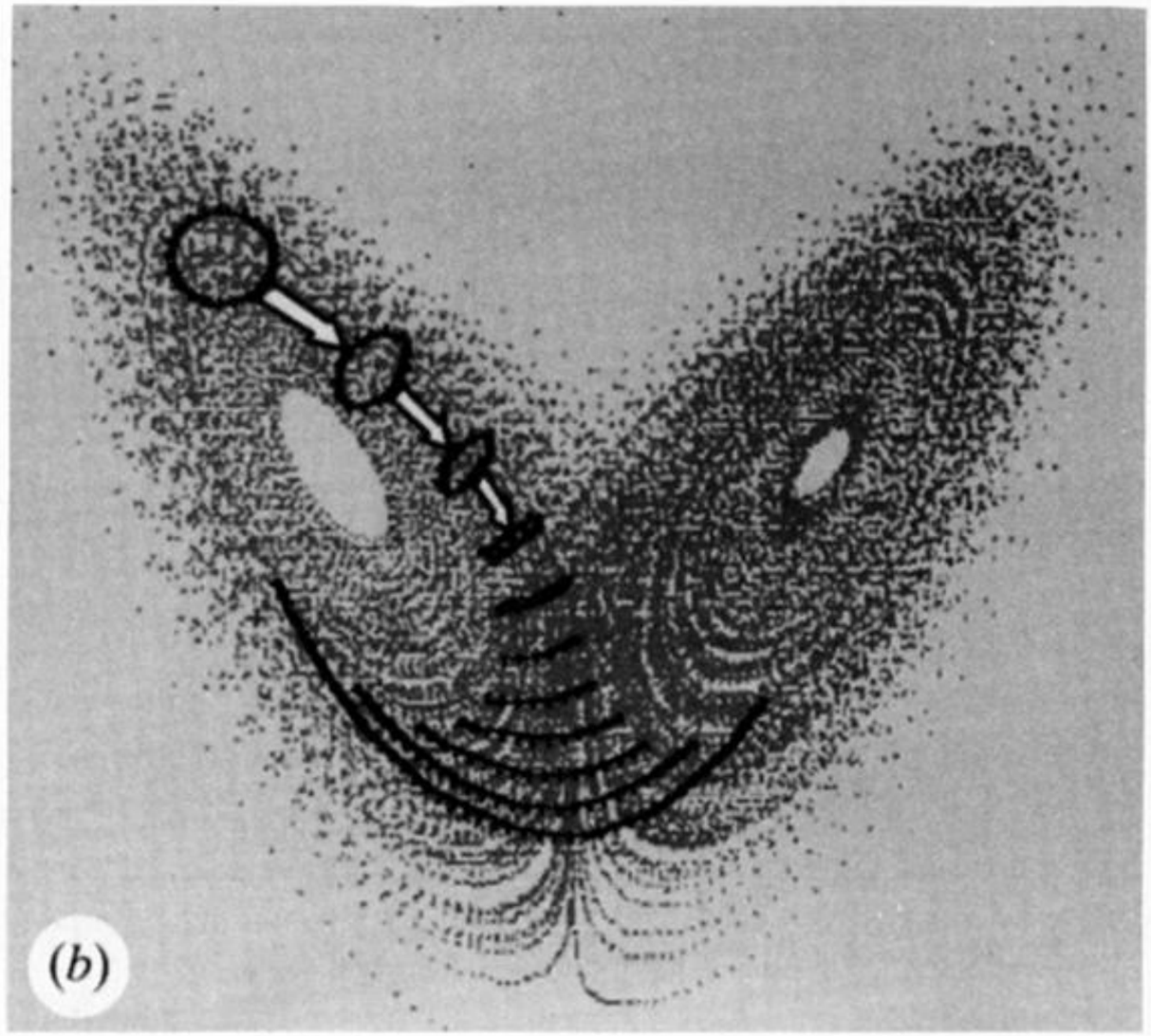

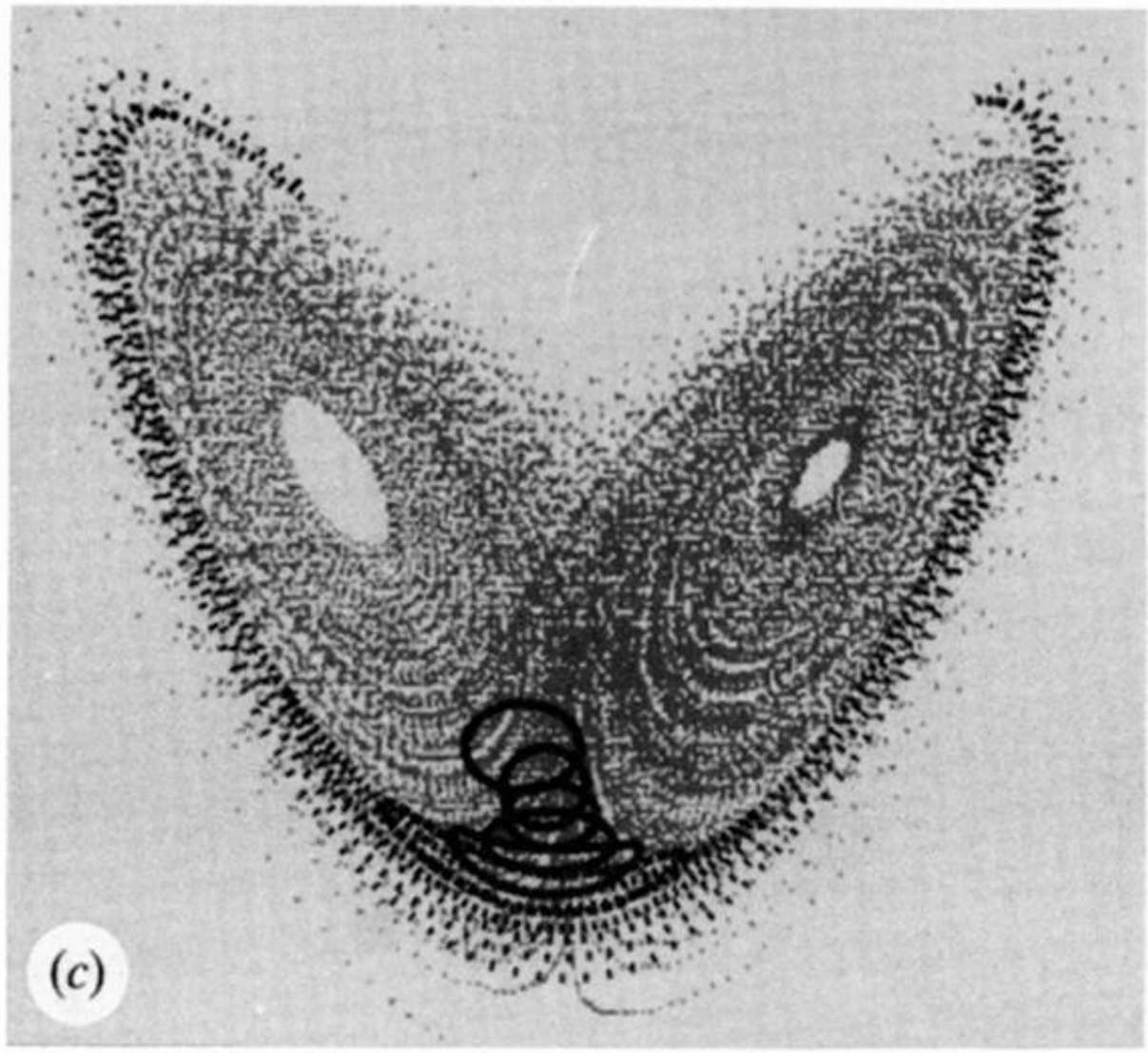

Figure 1. Phase-space evolution of an ensemble of initial points on the Lorenz attractor, for three sets of initial conditions.

PHILOSOPHICAL TRANSACTIONS OF THE ROYAL SOCIETY A MATHEMATICAL, PHYSICAL & ENGINEERING SCIENCES